JOURNAL OF APPLIED ELECTROCHEMISTRY **27** (1997) 805–814

Development of an inverted rotating shaft-disc electrode (IRSDE)

E. J. PODLAHA, A. BÖGLI, Ch. BONHÔTE, D. LANDOLT

Laboratoire de Métallurgie Chimique, Département des Matériaux, Ecole Polytechnique Fédérale de Lausanne, CH-1015 Lausanne, Switzerland

Received 20 August 1996

An alternative electrode design to existing inverted rotating disc electrode configurations is presented which eliminates the need for a special cell. A thin, insulated, conducting shaft is mounted in the centre of an electroactive disc. The resulting electrode, an inverted rotating shaft-disc electrode (IRSDE), can be mounted on any conventional disc rotator. Ferricyanide and copper reduction were used to characterize the mass transfer behaviour for different size disc electrodes with a constant shaft diameter. The limiting current was found to vary linearly with the square root of rotation rate for all sizes. The Levich equation was valid for a small shaft to disc radius. A maximum in the thickness of deposited copper near the central shaft was observed resulting from the combined effect of a radial component to mass transport and the shaft wall. An empirical expression for the average limiting current density at the IRSDE taking into account the shaft to disc radius ratio is presented.

1. Introduction

The active electrode surface of conventional rotating disc electrodes (RDE) faces downwards. As a consequence gas bubbles may become trapped at the electrode surface due to buoyancy forces. This can lead to measurement errors caused by partial blockage of the surface and to growth defects in electrodeposits. In the present paper a special type of inverted disc electrode facing upwards is presented which has the advantage of permitting a simple cell design while avoiding the problem of bubble entrapment.

The maximum reaction rate at a rotating disc is given by the Levich equation [1, 2]. The velocity distribution described by the Navier–Stokes and continuity equations were resolved by von Kármán [3] and Cochran [4], in the form of a serial expansion. Subsequently, Levich [1, 2] solved the convective-diffusion mass transport equation by using only the first term of the velocity serial expansion, valid for conditions where the kinematic viscosity, ν, is much greater than the diffusion coefficient, D. Such conditions are generally met for aqueous electrolytes. The resulting diffusional flux near the electrode surface is independent of electrode radius and the surface is considered to be uniformly accessible. If the central portion of the disc is made to be inactive, the resulting geometry corresponds to that of a rotating ring electrode (RRE). The radial mass transport component present leads to a higher reaction rate [2, 5–7] and to a nonuniform diffusion layer thickness.

Another assumption used in the solution of the Navier–Stokes equations is that forced convection greatly outweighs natural convection eliminating the gravitational term. Therefore, positioning the electrode either downwards or upwards in the solution should have no influence on convective mass transport. Indeed, it has been verified that the Levich equation holds also for an inverted rotating disc electrode (IRDE) [8, 9]. Unfortunately, the implementation of the IRDE configuration requires an elaborate cell design to avoid leakage. Zdunek and Selman [8] proposed a cell assembly where the IRDE enters the working electrode compartment through a hole at the bottom of the cell. A stationary seal was used to avoid leakage of the electrolyte while allowing the electrode to rotate. Bressers and Kelly [9] avoided the sealing problem by rotating the entire cell including the disc electrode. A stationary inner cylinder was placed concentric to the disc electrode to reduce electrolyte convection.

In the present study an alternative electrode design is presented, the inverted rotating shaft–disc electrode (IRSDE). A thin shaft, electrically conducting and surrounded by an insulator, is connected to a flat, circular disc electrode facing upwards as shown in Fig. 1(a). The IRSDE can easily be mounted in existing RDE rotator assemblies and introduced into any conventional cell. Rotating discs with a central shaft of the type shown in Fig. 1(b) and (c) have been described previously in the literature with the objective of validating the Levich equation [10, 11]. The electrode area in both these configurations included the upper and lower surfaces of the electrode as well as the side wall. Siver and Kabanov [10] found a deviation from the Levich behaviour using the configuration shown in Fig. 1(b). Heitz [11] observed that with a design as in Fig. 1(c) good agreement to the Levich equation was possible when the shaft radius was made much smaller than the disc radius. This configuration has been used for corrosion applica-

0021-891X

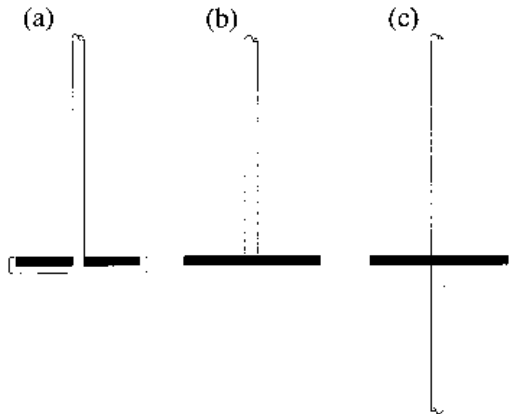

Fig. 1. Various shaft electrode designs: (a) only the top surface is electroactive with the central shaft connected to one face of the disc, (b) all electrode surfaces are electroactive with the shaft connected to one face of the disc, (c) all electrode surfaces are electroactive with the shaft in the middle of both the upper and lower surface.

tions [12–14]. In the IRSDE presented in this paper the active electrode area is restricted to the upper side of the disc. The IRSDE is not a true disc nor a true ring electrode and the mass transport distribution is expected to be influenced by the central shaft. In the present paper mass transport at the IRSDE is compared to that at the RDE for various values of disc radius with the aim of developing a new tool for the study of electrochemical phenomena.

2. Experimental details

2.1. *IRSDE design*

A schematic of the electrode design is shown in Fig. 2. Stainless steel disc electrodes (AISI 304L) were embedded into an epoxy resin (Araldite®) so that only one side of the metal disc is exposed to the electrolyte. The diameter of the insulating region was 0.2 cm larger than the disc diameter and the thickness was 0.4 cm. A thin, stainless steel shaft, encased in Teflon, was screwed into the disc–epoxy assembly. The threaded shaft enabled electrical contact to the disc while also allowing electrodes to be interchangeable. The outer diameter of the shaft was 0.7 cm and the length was 6 cm. Four different size electrodes were examined having diameters of 4, 3, 2 and 1cm and the results were compared to a conventional RDE, 0.4 cm diameter.

2.2. *Ferricyanide ion reduction*

Ferricyanide reduction from a basic electrolyte was studied due to the ability to easily observe distinct limiting current plateaus. The solution contained 0.1 M $K_3Fe(CN)_6$ and 1 M KOH. The temperature was maintained at 25 °C by means of a thermostated water bath. A single compartment, double jacketed glass cell was employed containing approximately 0.75 dm^3 of solution. The anode was a platinum mesh

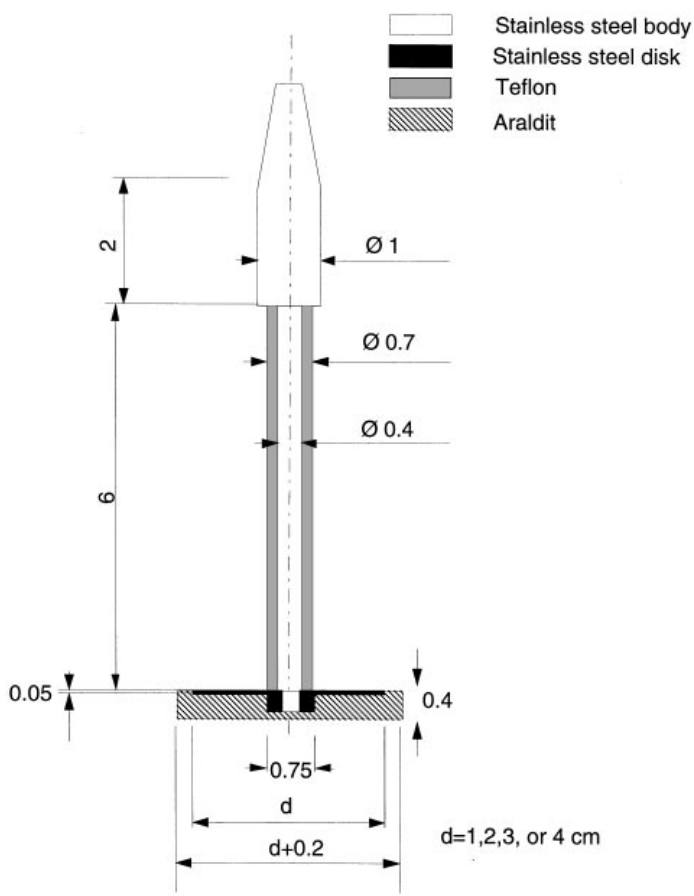

Fig. 2. IRSDE schematic. Dimensions in cm.

and a calomel reference electrode SCE (0.2412V vs NHE), placed about 1 cm above the edge of the disc. The stainless steel IRSDE cathode surface was polished and cleaned with an ultrasonic treatment prior to each experiment. Linear sweep voltammetric measurements at different rotation rates were carried out at $5\,mV\,s^{-1}$ in all experiments with an Autolab, Eco Chemie potentiostat.

2.3. *Cupric ion reduction*

Copper deposition was chosen for the study of the radial current distribution on the IRSDE by measuring the deposit thickness as a function of radial distance. An acid electrolyte consisting of 0.05 M $CuSO_4$ and 1 M H_2SO_4 deaerated with nitrogen was used at 25 °C. The cell configuration was the same as in the ferricyanide experiments except for the use of a copper anode and a saturated mercury sulfate reference electrode (MSE) having a potential of 0.64 V vs NHE. The reference electrode was placed in a fixed position 3.5 cm away from the centre of the insulating shaft of the IRSDE and the ohmic drop was measured by impedance spectroscopy (Zahner). The ohmic drop was 0.3, 0.4, 0.65, 1.7 and 4 Ω for the 4, 3, 2, 1 IRSDE and RDE, respectively. Due to the poor adhesion of copper on stainless steel a thin layer of gold was plated on the IRSDE electrode surface in some experiments, using a commercial electrolyte (Autostrike II, Lea Ronal). Polarization curves were measured in the same manner as in the ferricyanide reduction experiments. Potentiostatic measurements were carried out at the limiting current for 120 s at various rotation rates and electrode sizes. The copper thickness was measured using X-ray fluorescence (Kevex) taking into account the substrate composition as well as the additional gold layer. The conditions used for the X-ray fluorescence were 300 μm collimator, 30 kV, 0.1 mA, and 60 s acquisition time in an air environment. An electrochemical stripping technique was used as an independent method to confirm the validity of the X-ray fluorescence results. (See Appendix.)

3. Results

Typical polarization curves for the reduction of ferricyanide on the 3 cm diameter IRSDE are shown in Fig. 3 for different rotation rates. The curves were not corrected for ohmic drop since only the value of the limiting current is of interest here. Similar limiting current plateaus were found for the different size electrodes. Figure 4 shows the inverse of the limiting current density as a function of the inverse of the square root of the rotation rate for the four IRSDE of different size and for the conventional RDE. The coefficients corresponding to the linear regression lines shown in the figure are presented in Table 1. A linear dependency of the limiting current on the square root of rotation rate is noted for all the IRSDE with high correlation coefficients. As the size of the IRSDE becomes bigger (at constant shaft radius) the slope of the Levich plot approaches that of the RDE.

Examples of polarization curves for the copper system are shown in Fig. 5 for polished and for gold coated stainless steel substrates, respectively. Ap-

Table 1. Ferricyanide reduction linear regression of Fig. 4

IRSDE size /cm	*Slope* / $mA^{-1}\,cm^2\,rpm^{0.5}$	*Intercept* / $mA^{-1}\,cm^2$	*r*
1	0.5369	−0.000 242 71	0.999 27
2	0.650 26	−0.000 263 62	0.999 84
3	0.678 86	−0.000 260 21	0.998 89
4	0.664 04	0.000 383 54	0.999 62
RDE	0.714 17	−0.000 096 88	0.999 62

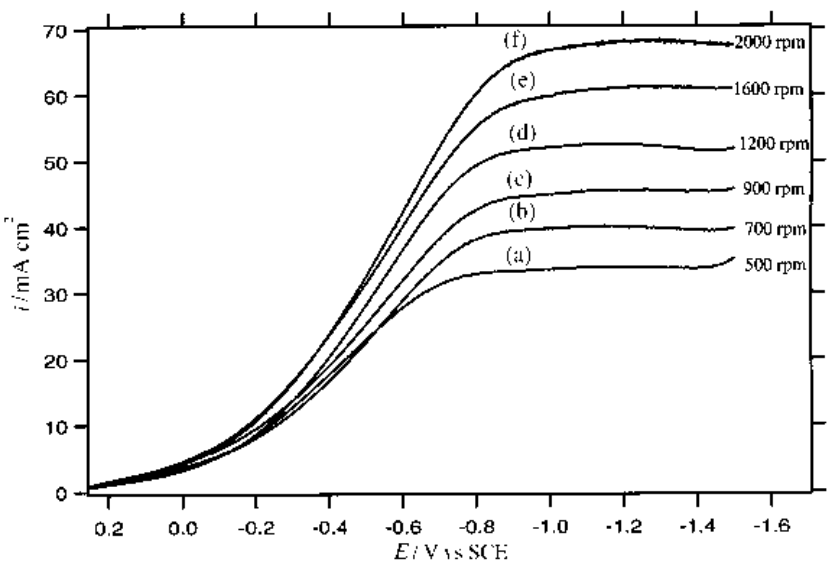

Fig. 3. Ferricyanide ion reduction polarization curves at different rotation rates for a 3 cm diameter IRSDE: (a) 500, (b) 700, (c) 900, (d) 1200, (e) 1600 and (f) 2000 rpm.

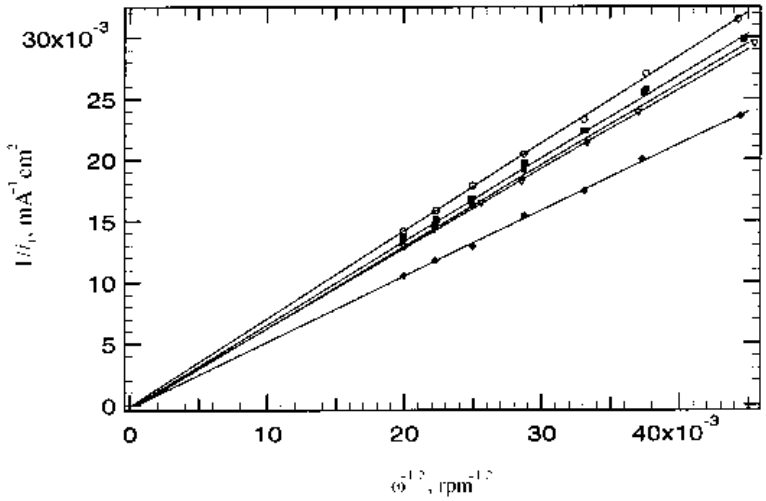

Fig. 4. Ferricyanide ion reduction inverse Levich plot. IRSDE diameter: (◆) 1, (▽) 2, (●) 3 and (■) 4 cm; (○) RDE. Solid lines represent the linear regression of the data.

proximately the same limiting current value is found for the two substrate surfaces but the gold coating significantly affects the kinetic regions of both the copper and hydrogen evolution reactions. After the polarization curve was completed the copper deposit on the stainless steel surface was powdery and non-adherent. In contrast, the copper deposited on the gold surface was firmly attached to the substrate. Although the surface morphology of the deposited copper tended to be slightly dendritic if the layer was thick (several micrometres), it was not powdery as in the case when the stainless steel surface was used. Thus the gold surface was used for most experiments except at high rotation rates when for kinetic reasons the limiting current was better defined with the stainless steel substrate.

During polarization at large overpotentials gas bubbles were observed in the acid copper electrolyte. These did not adhere and freely detached from the electrode surface. On the other hand, when copious gas generation occurred the bubbles tended to stick onto the insulating regions of the electrode holder, that is, the central Teflon shaft and the epoxy ring.

The inverse Levich plot for cupric ion reduction, in Fig. 6, shows a similar behaviour as for the ferricyanide reduction. The linear regression coefficients corresponding to the data points for different electrode sizes are given in Table 2. The larger the IRSDE the closer is the behaviour to a true RDE. For a purely mass transport controlled process the inverse Levich plot should go through zero but in Fig. 6 a slight deviation is observed. This nonzero intercept is due to a kinetic contribution, and also reflects the difficulty in the copper sulfate electrolyte to clearly identify the limiting current which can be partially obscured by the side reaction, particularly at

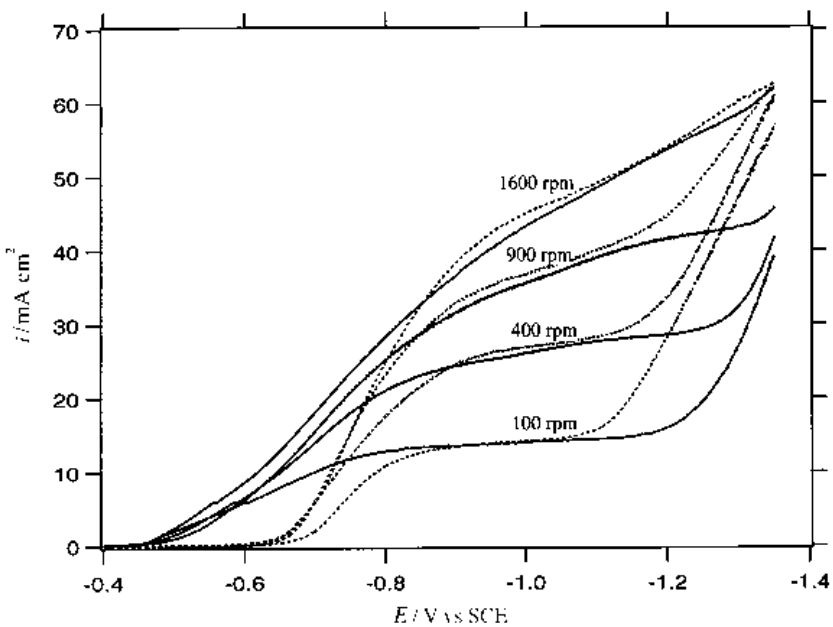

Fig. 5. Sample cupric ion reduction polarization curves at different rotation rates, comparing a stainless steel (·····) and gold electrode (——) surface. IRSDE diameter: 3 cm.

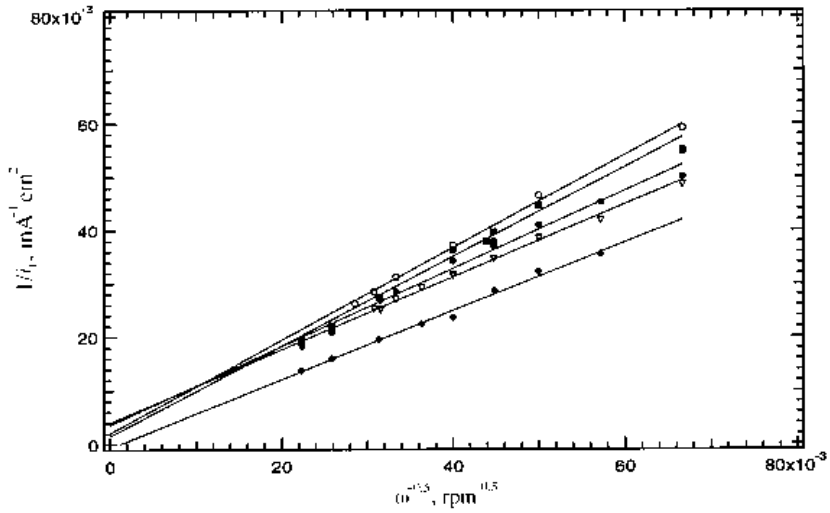

Fig. 6. Inverse Levich plot of the cupric ion reduction. IRSDE diamter: (◆) 1, (▽) 2, (●) 3 and (■) 4 cm; (○) RDE. Solid lines represent the linear regression of the data.

high rotation rates. Additionally, copper is continually depositing on the electrode surface during the duration of the polarization scan and resulting changes in electrode area could also be reflected in the Levich plots.

The thickness distributions of copper deposited potentiostatically on the gold surface are shown in Fig. 7 for different electrode sizes at a constant rotation rate of 400 rpm as a function of radial position r. The outer edge of the IRSDE is located at the disc radius, $r = r_d$, and the centre of the shaft is at $r = 0$. The applied potential was chosen to be approximately in the middle of the limiting current plateaus, −0.8, −0.95, −1.1, −0.9 V vs MSE for the 1, 2, 3 and 4 cm diameter IRSDE, respectively. The three largest IRSDEs all show a constant deposit thickness away from the central rotating shaft. There is an increase in the deposit thickness near the shaft followed by an abrupt decrease. Unfortunately, it is difficult to resolve the thickness very close to the shaft since the X-ray fluorescence technique provides an average thickness over the excited microspot region. For the collimator used here this averaging region is an ellipse having the size of 0.045 cm for the major axis and 0.032 cm for the minor axis. The influence of rotation rate on the deposit thickness is shown in Fig. 8 for the 2 and 4 cm diameter IRSDE, respectively. In all cases there is a large region of uniform thickness and a perturbed region near the shaft. The increase in average thickness with rotation rate follows the square root dependence for both size electrodes.

Table 2. Copper reduction linear regression of Fig. 6

IRSDE size /cm	*Slope* / mA^{-1} cm^2 $rpm^{0.5}$	*Intercept* / mA^{-1} cm^2	*r*
1	0.640 86	−0.000 716 67	0.996 09
2	0.680 63	0.004 046 6	0.993 99
3	0.730 35	0.003 637 2	0.991 75
4	0.830 69	0.001 419 13	0.994 59
RDE	0.867 13	0.002 093 8	0.998 47

4. Discussion

The Levich equation describes the limiting current density for the RDE:

$$i_{l,RDE} = 0.62\, nFD^{2/3}\nu^{-1/6}\omega^{1/2}C \qquad (1)$$

The limiting current density of the RRE is given by Equation 2 which corresponds to that for the RDE

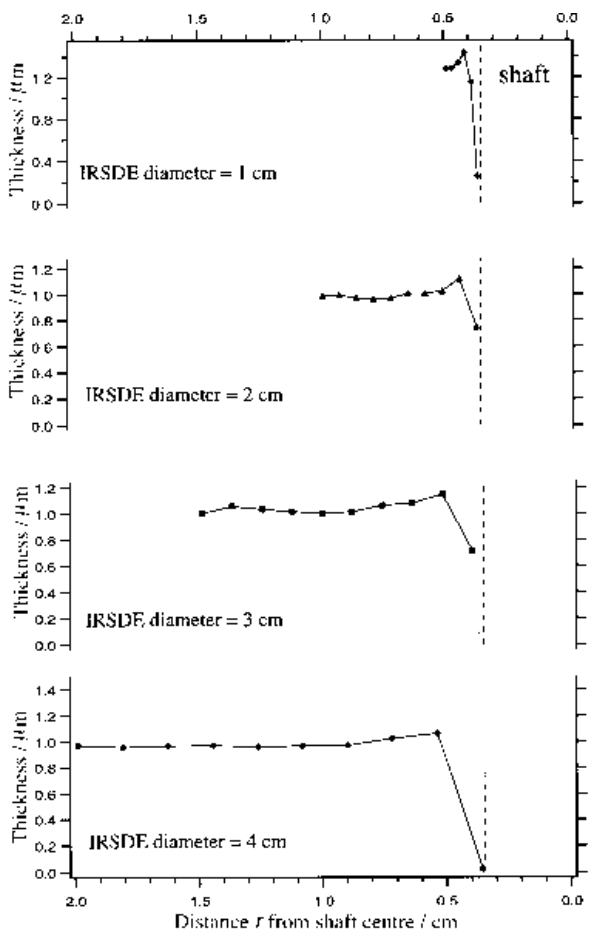

Fig. 7. Copper thickness distribution for different size IRSDE plated at the limiting current for 120 s at 400 rpm.

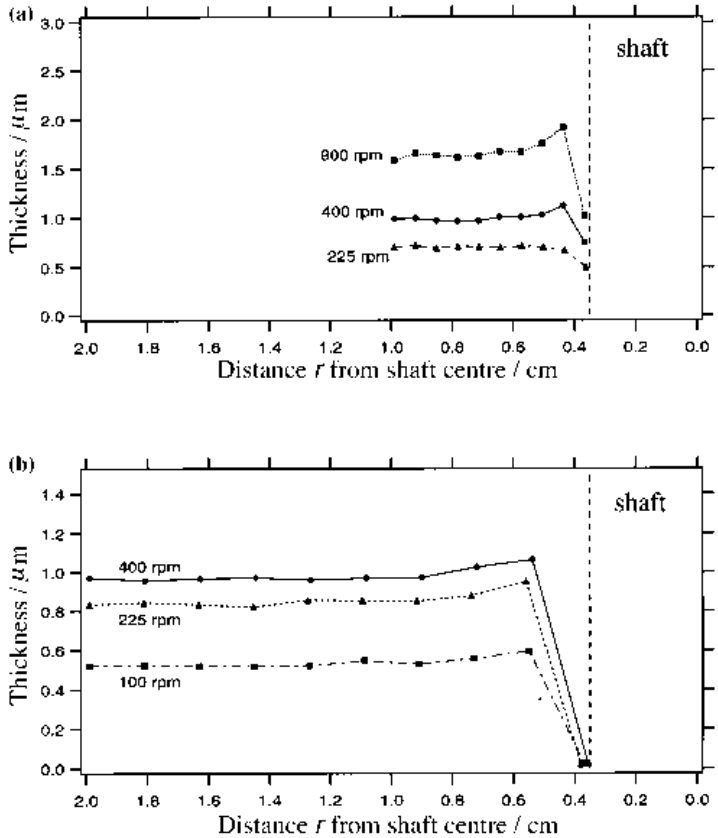

Fig. 8. Deposit thickness at different rotation rates for the IRSDE having a diameter of (a) 2 and (b) 4 cm, plated at the limiting current for 2 min.

but contains an additional term which is dependent on the ring size [2, 5–7]:

$$i_{l,RRE} = 0.62\,nFD^{2/3}\nu^{-1/6}\omega^{1/2}C\frac{(r_2^3 - r_1^3)^{2/3}}{r_2^2 - r_1^2} \qquad (2)$$

Here r_1 and r_2 are the radius of the inner insulating disc and outer conducting annulus. For a constant central insulating disc size, as the ring becomes thinner, r_2 becomes smaller, and the limiting current density increases. If the ring becomes very large so that $r_2 \gg r_1$ then the RRE behaves as an RDE.

The average mass transfer rate of the IRSDE depends essentially on two parameters, the angular velocity ω and the ratio of the shaft to disc radius $a = r_s/r_d$. Due to the hydrodynamics of disc electrodes a linear dependence of the average limiting current of the IRSDE with the square root of angular velocity should be expected. On the other hand, the central shaft may create a turbulent region similar to rotating cylinder electrodes which could lead to another rotation rate dependence near the inner edge of the IRSDE. Figure 9 shows the inverse of the average limiting current measured on IRSDE normalized to that of the RDE and the RRE, respectively, as a function of $\omega^{-1/2}$. The linear regression data of Table 1 was used to calculate the limiting currents of the RDE and RRE by Equations 1 and 2. The normalized limiting currents of Fig. 9 are constant for all electrode sizes studied. This confirms that the central shaft did not influence the rotation rate dependence of the average limiting current.

In Fig. 10 the limiting currents for ferricyanide reduction on the IRSDE normalized to those on the RDE and RRE, respectively, are plotted as a function of the radius ratio a. Also shown is the ratio $i_{l,RRE}/i_{l,RDE}$. From Equations 1 and 2 this ratio is given by

$$\frac{i_{l,RRE}}{i_{l,RDE}} = \frac{(r_2^3 - r_1^3)^{2/3}}{r_2^2 - r_1^2} \qquad (3)$$

When $a > 0$ the ratios $i_{l,RRE}/i_{l,RDE}$ and $i_{l,IRSDE}/i_{l,RDE}$ are always greater than one due to the presence of a radial component which enhances mass transport. At low values of a the limiting current density on the IRSDE is nearly the same as that on the RRE while at high values of a it becomes smaller as the effect of the shaft becomes increasingly important.

The RRE is inherently not a uniformly accessible electrode surface, unlike the RDE. Due to the central inert region fresh solution is continually supplied to the inner edge of the ring thus inducing a radial flux of species. The local, reaction rate distribution is given by Levich:

$$i_{RRE}(r) = i_{RDE}\left(1 - \frac{r_1^3}{r^3}\right)^{-1/3} \qquad (4)$$

Similarly, the copper deposition results in Figs 7 and 8 reveal a radial flux contribution. However, no analytical solution for the limiting current distribution on the IRSDE is available and therefore it was determined experimentally. The local limiting current density on the IRSDE was determined from the

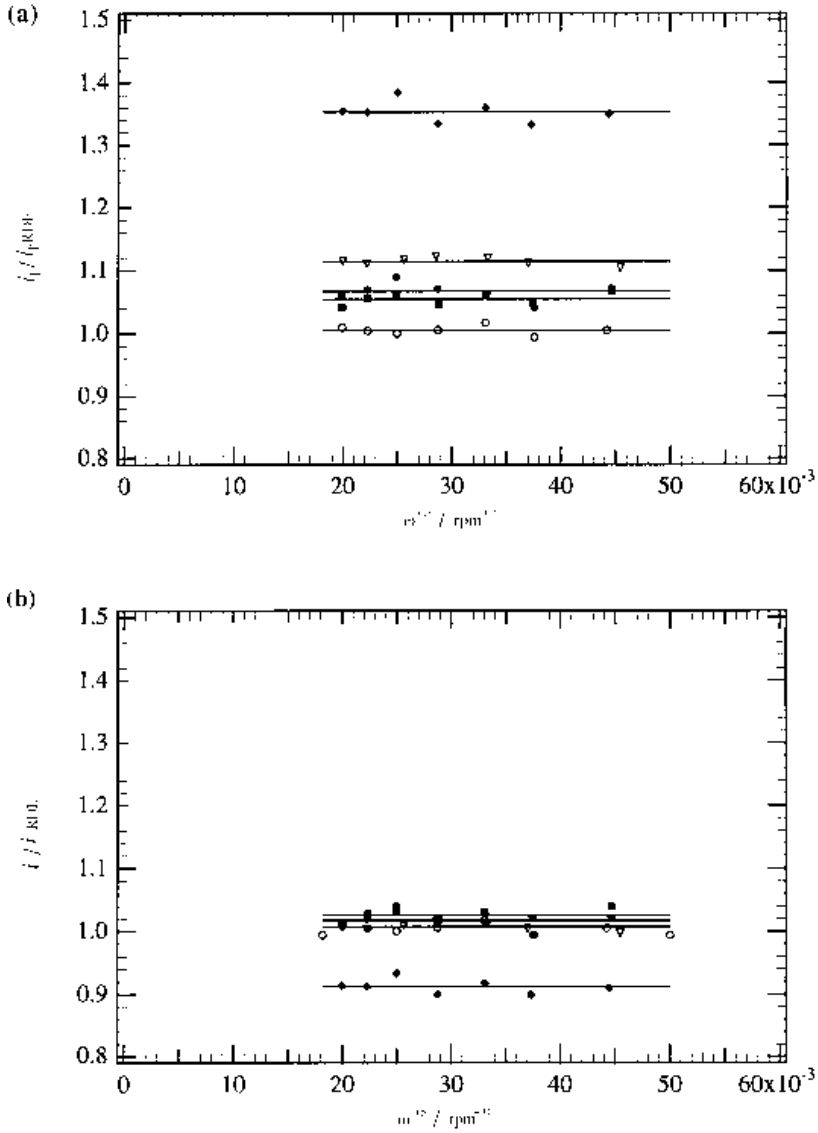

Fig. 9. Normalized IRSDE limiting current density with (a) a RDE and (b) RRE having the same size electrode as a function of the inverse square root of angular velocity. IRSDE diameter: (◆) 1, (▽) 2, (●) 3 and (■) 4 cm; (○) RDE; (——) average.

thickness of the copper deposits and compared to Equation 4. In Fig. 11 the measured local limiting currents are normalized to the average value, integrated over the electrode area. The experimental data are those presented in Fig. 7 for a rotation rate of 400 rpm. In the case of a true RDE the local thickness should be the same everywhere (neglecting edge effects). For the RRE, Equation 4 predicts an infinite limiting current density at the inner edge of the ring electrode and a decrease towards the outer edge. The data of Fig. 11 show that for the IRSDE the presence of the shaft leads to a sharp drop of limiting current in its immediate vicinity. The electrolyte solution at the inner border apparently is not readily renewed because of the presence of the shaft. A maximum in the local deposit thickness is observed at about 0.1 cm away from the shaft wall. This suggests that two opposing effects determine the mass transport conditions at the IRSDE. On the one hand the shaft inhibits electrolyte renewal near the vertical wall, while on the other hand a radial flux component increases the rate of transport at some distance from the shaft. The data of Fig. 8 indicate that this localized behaviour is influenced only by the rotation rate of the disc ($\omega^{-1/2}$) and is practically insensitive to the hydrodynamics of the cylindrical shaft.

Based on the described behaviour, an expression can be proposed for the prediction of the average limiting current density on the IRSDE. The thickness distribution measurements reveal that the local reaction rate is enhanced towards the inner electrode boundary, similar to the RRE, but at the border of the rotating shaft the reaction rate is greatly reduced. Thus, an equation of the same form as Equation 2 for the RRE is used to describe mass transport at the IRSDE however, an effective inner radius $r_{s,eff}$ bigger than the shaft radius r_s replaces r_1. The use of an effective inner radius accounts for the loss of local reaction rate near the shaft boundary. The value of $r_{s,eff}$ was determined by fitting the ferricyanide experimental data obtained with the smallest diameter disc of 1 cm. This electrode size corresponded to the largest a value studied here and therefore exhibited the biggest deviation from both the RRE and RDE

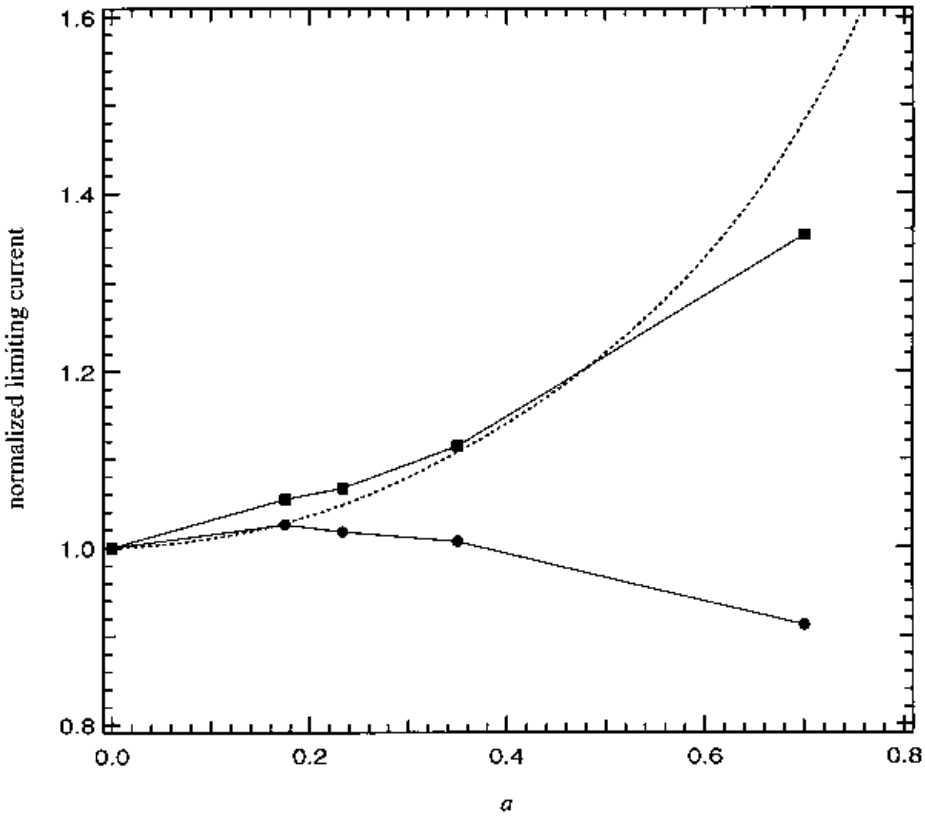

Fig. 10. Normalized IRSDE ferricyanide ion reduction limiting current density to that of a RDE and RRE as a function of dimensionless radius. A comparison between the limiting current of the RRE and RDE ($i_{l,RRE}/i_{l,RDE}$) is also shown as the dashed line. Key: (■) $i_l/i_{l,RDE}$ and (●) $i_l/i_{l,RRE}$.

limiting currents. A reasonable fit was found for an effective radius of $r_{s,eff} = 1.075\, r_s$. Therefore, the empirical Equation 5 describes the average limiting current for the range of IRSDE geometries studied here.

$$i_{l,IRSDE} = i_{l,RDE} \frac{\left(r_d^3 - [1.075 r_s]^3\right)^{2/3}}{r_d^2 - r_s^2} \qquad (5)$$

The predictions of Equation 5 are compared in Fig. 12 to the ferricyanide data and Fig. 13 to the copper deposition data. Good correspondence is observed for both systems.

Although, the IRSDE is a simple alternative for the inverted RDE some limitations should be mentioned. To approach the true Levich behaviour the ratio a must be small. This requirement can lead to relatively large electrode areas and a corresponding need for a high current power supply and a cell of rather large volume. For example, according to Fig.10 for $a = 0.2$ the deviation from the Levich (Equation 1) is of the order of 5%. For the shaft

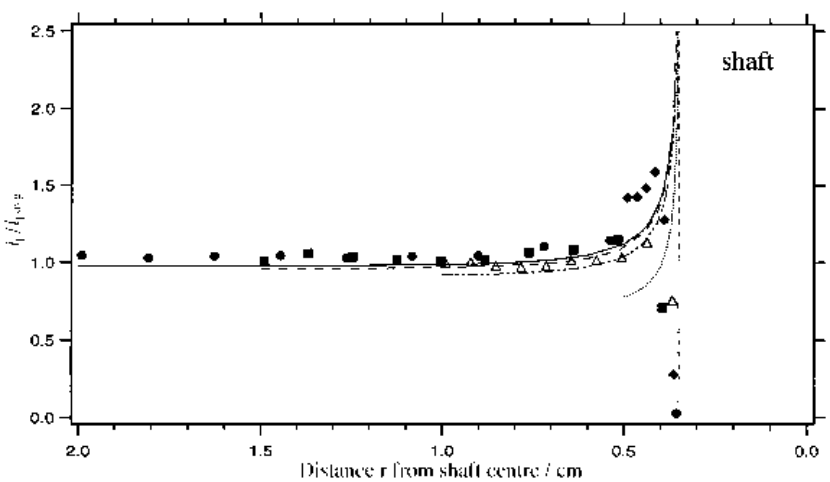

Fig. 11. Normalized local to average current density as a function of the local electrode position for different IRSDE sizes: (◆) 1, (△) 2, (■) 3 and (●) 4 cm. Also, theoretical thickness distribution predicted by the equation for a RRE with $r_1 = 0.35$ cm and r_2: (——) 2.0, (- - -) 1.5, (–···) 1.0 and (·····) 0.5 cm.

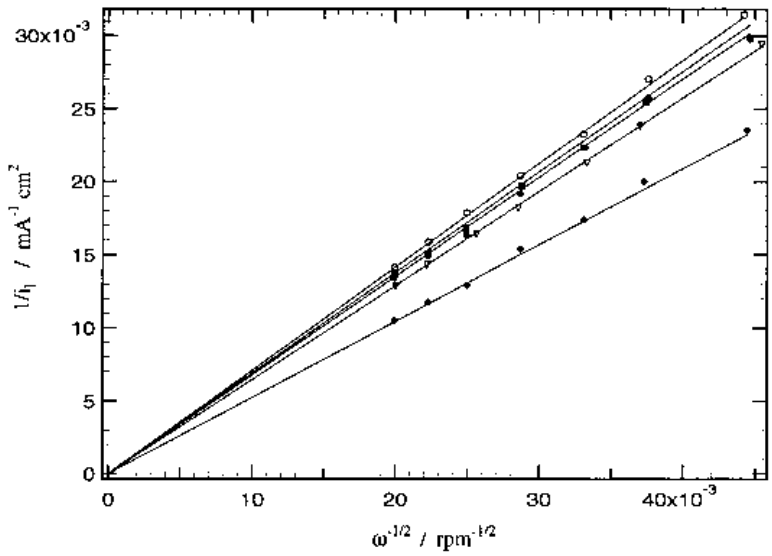

Fig. 12. Predicted IRSDE limiting current determined from Equation 5 compared to the ferricyanide ion reduction data. IRSDE diameter: (◆) 1, (▽) 2, (●) 3 and (■) 4 cm; (○) RDE and (——) prediction.

radius of 0.35 cm chosen here, this leads to an active electrode area of 37 cm^2. The shaft diameter could probably be made smaller but there is a limit to this because the mechanical stability must remain sufficient to avoid eccentricities of the rotating electrode. The IRSDE dimensions chosen here were a compromise between these different considerations.

5. Conclusions

The IRSDE (inverted rotating shaft disc electrode) is a simple rotating electrode system which has similar characteristics as the inverted rotating disc electrode without the need for a special cell design and sealing. It allows one to avoid problems due to adherence of gas bubbles when performing electrochemical studies under controlled mass transport conditions. Mass transport at the IRSDE over a wide range of conditions can be described by an equation similar to that of the rotating ring electrode where the inner radius is replaced by an effective radius. The use of an effective inner radius accounts for the fact that the rate of mass transport at the inner edge of the active electrode surface is decreased by the presence of the shaft. For small values of the shaft to disc radius ratio, the average limiting current density of the IRSDE approaches that predicted by the Levich equation for a rotating disc electrode.

Acknowledgements

The authors would like to thank L. Masson for his helpful suggestions concerning the design of the IRSDE and acknowledge the Fonds National Suisse pour la Recherche Scientifique for financial support.

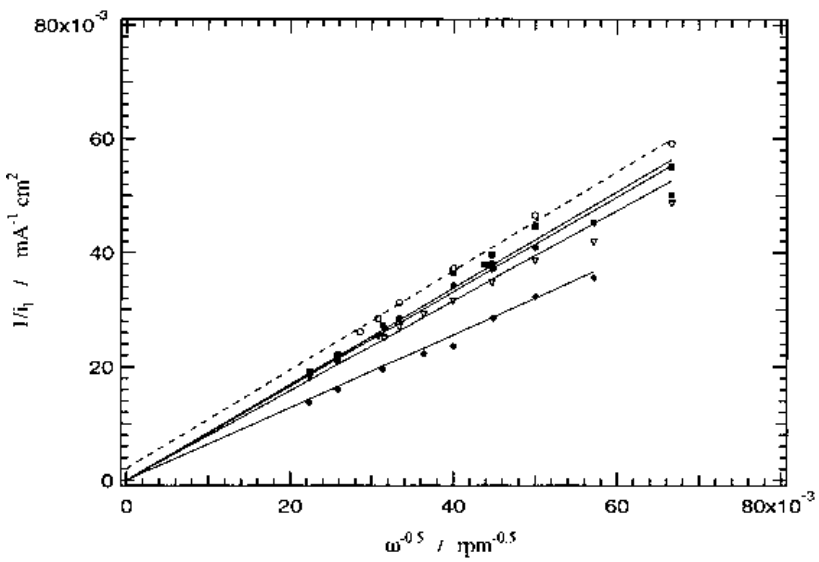

Fig. 13. Predicted IRSDE limiting current determined from Equation 5 compared to the cupric ion reduction data. IRSDE diameter: (◆) 1, (▽) 2, (●) 3 and (■) 4 cm; (○) RDE, (-----) RDE linear regression; (——) prediction.

References

[1] V. G. Levich, *Acta Physicochim. (URSS)*, **17** (1942) 257.
[2] V. G. Levich, 'Physicochemical Hydrodynamics', Prentice-Hall, Englewood Cliffs, NJ (1962), p. 314.
[3] T. von Kármán, *Z. Angew. Math. Mech.* **1** (1921) 233.
[4] W. G. Cochran, *Proc. Cambridge Phil. Soc.* **30** (1934) 365.
[5] N. Ibl, *J. Electrochem. Soc.* **108** (1961) 610.
[6] A. C. Riddiford, *in* 'Advances in Electrochemistry and Electrochemical Engineering', vol. 4., Interscience, New York (1966), pp. 47–116.
[7] A. J. Arvia and S. L. Marchiano, *in* 'Modern Aspects of Electrochemistry', vol. 6., Interscience, New York (1971) pp. 159–241.
[8] A. D. Zdunek and J. R. Selman, *J. Electrochem. Soc.* **139** (1992) 2549.
[9] P. M. M. C. Bressers and J. J. Kelly, *ibid* **142** (1995) L114.
[10] G. Yu. Siver and B. N. Kabanov, *Zh. Fiz. Khim. (Russia)* **22** (1948) 53.
[11] E. Heitz, Paper presented at 14th meeting C.I.T.C.E. Moscow (1963), *in* 'Advances in Electrochemistry and Electrochemical Engineering', (edited by A.C. Riddiford) vol. 4., Interscience, New York (1966), pp. 47–116.
[12] E. Heitz, *Werkst. Korros.* **15** (1964) 63.
[13] *Idem*, *ibid.* **10** (1965) 49.
[14] F. Franz, E. Heitz, G. Herbsleb and W. Schwenk, *ibid.* **24** (1973) 97.

Appendix

The calibration of the X-ray fluorescence was performed with bulk samples of thick copper which is interpreted as an infinite thickness. The local thickness measurement is thus calculated by the intensity of the X-ray signal emitted. Gravimetry analysis can be performed to verify the calibration when the deposit mass is large enough to yield a reliable weight measurement, but when there is only a thin deposit layer and the electrode size is small the change in mass approaches the limit of conventional scales. In this study copper has a tendency to form dendrites when the deposit thickness is several micrometres, therefore the thickness was kept on the order of 1 μm.

The gold RDE was used to check the calibration of the X-ray fluorescence for the copper thickness since it should have a nearly uniform current distribution at the limiting current. Deposition was carried out at the limiting current for two minutes keeping the deposit thickness near 1 μm. In order to account for current efficiencies that may not be 100% a stripping procedure was used to measure the amount of anodic charge, Q, which occurs during the oxidation of the solid copper to the cupric ion. The stripping curves are shown in Fig. 14(a) for samples plated with copper at different rotation rates, for 120 s at a constant potential of –0.85 V vs MSE. The rotation rate during stripping was 2000 rpm. The same acid copper sulfate bath was used for both plating and stripping. During stripping the potential, uncorrected for ohmic drop, was swept from the equilibrium potential to an anodic potential at 5 mV s^{-1}. The scan was ended

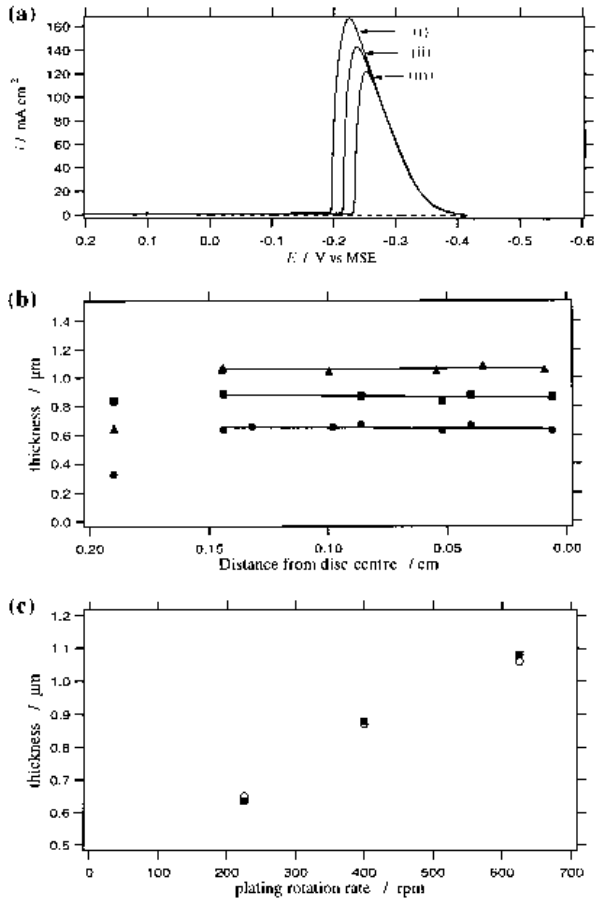

Fig. 14. (a) Stripping voltammetry used to calculate the copper deposit thickness from the stripping charge. The copper stripping curves are shown as the solid curves for different plating rotation rates, while the gold substrate is presented as the dashed line: (i) 625 rpm, (ii) 400 rpm, (iii) 225 rpm. (b) Copper thickness measurement obtained from X-ray fluorescence for deposits plated at the limiting current at three different rotation rates. (●) 225 rpm, (■) 400 rpm, (▲) 625 rpm. (c) A comparison of the measured thickness from the X-ray fluorescence technique (○) and the electrochemical stripping method (■).

when it was clear that the electrode did not have any more copper on it. The thickness, Δt, was determined through Faraday's law

$$\Delta t = \frac{QM}{nF\rho\pi r^2} \qquad \text{(A1)}$$

where ρ is the density of copper and M is the molecular weight.

The thickness distribution measured by X-ray fluorescence, in Fig. 14(b), shows a uniform thickness over the radius of the RDE as expected, except near the outer edge of the electrode. The average value is shown as a straight line.

Fig. 14(c) shows the comparison of the two techniques. The stripping results agree fairly well with the X-ray fluorescence and gives confidence to the results presented here for the IRSDE.